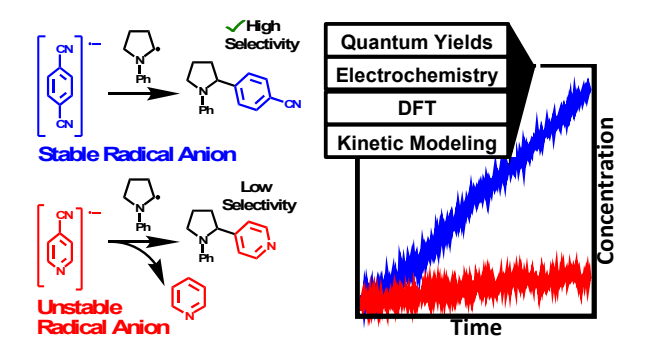
# **Photoredox Product Selectivity Controlled by Persistent Radical Stability**

Bernard G. Stevenson<sup>†1</sup>, Cameron Gironda<sup>†1</sup>, Eric Talbott<sup>1</sup>, Amanda Prascsak<sup>2</sup>, Nora L. Burnett<sup>1</sup>, Victoria Kompanijec<sup>1</sup>, Roman Nakhamiyayev<sup>1</sup>, Lisa A. Fredin\*<sup>2</sup> and John R. Swierk\*<sup>1</sup>

- 1. Department of Chemistry, State University of New York at Binghamton, Vestal, NY 13850
- 2. Department of Chemistry, Lehigh University, Bethlehem, PA 18015 †Equal contributions



ABSTRACT: The use of photoredox catalysis for the synthesis of small organic molecules relies on harnessing and converting the energy in visible light to drive reactions. Specifically, photon energy is used to generate radical ion species that can be harnessed through subsequent reaction steps to form a desired product. Cyanoarenes are widely used as arylating agents in photoredox catalysis because of their stability as persistent radical anions. However, there are marked, unexplained variations in product yields when using different cyanoarenes. In this study, the quantum yield and product yield of an α-aminoarylation photoredox reaction between five cyanoarene coupling partners and N-phenylpyrrolidine were characterized. Significant discrepancies in cyanoarene consumption and product yield suggested a chemically irreversible, unproductive pathway in the reaction. Analysis of the side products in the reaction demonstrated the formation of species consistent with radical anion fragmentation. Electrochemical and computational methods were used to study the fragmentation of the different cyanoarenes and revealed a correlation between product yield and cyanoarene radical anion stability. Kinetic modeling of the reaction demonstrates that cross-coupling selectivity between N-phenylpyrrolidine and the cyanoarene is controlled by the same phenomenon present in the persistent radical effect.

### INTRODUCTION.

Visible light photocatalysis is used to drive different types of small molecule, bond-forming transformations. 1-8 Photocatalytic transformations harness the oxidation or reduction potential of short-lived excited states that can undergo single electron transfer (SET), via reductive or oxidative quenching of excited state, to generate radical intermediates in redox-labile substrates. 9-13 Often, transition metal photocatalysts, like tris(2phenylpyridine)iridium (III) $(Ir(ppy)_3)$ tris(bipyridine)ruthenium(II) chloride ([Ru(bpy)<sub>3</sub>]<sup>2+</sup>), are used because of their longlived excited states, good visible light absorption, and tunable reduction potentials.<sup>14</sup> Organic photocatalysts have also received significant attention due to the lack of precious metals and ability to drive a wide range of transformations, however, many of these photocatalysts exhibit shorter excited state lifetimes, and care must be taken in reaction design.<sup>15,16</sup>

Careful design of the radical-generating SET event is necessary when developing photocatalytic transformations. <sup>17,18</sup> Depending on the mechanism of quenching, the SET event generates a radical cation or radical anion intermediate, which are inherently less stable than their neutral counterparts. <sup>19</sup> The added electron generally decreases the bond order of the substrate, decreasing bond strength. <sup>20,21</sup> In many cases, the decrease in bond strength can be leveraged to direct subsequent reaction steps. For example, photochemical reduction of aryl halides leads to a rapid fragmentation to generate the aryl

radical and halide anion.  $^{22}$  Alternatively, the  $\alpha$ -amino position in amine radical cations becomes significantly more acidic when compared to the neutral molecule and is readily deprotonated to give a neutral radical species.

Cyanoarenes are widely used as arylating agents in various photoredox reactions. 23-33 When reduced. the cyanoarene radical intermediates are considered to be long-lived "persistent" radicals, and that stability enables radical cross-coupling.<sup>34,35</sup> Though the cyano groups are strongly electron-withdrawing they are poor electron acceptors and the electron density is localized on the aromatic ring and not on the cyano group. 36,37 Though generally assumed to be stable, there are some reports of cyanoarene radical anions undergoing hydrogen addition or C-CN bond cleavage after reduction.<sup>38-40</sup>

A prototypical reaction using cyanoarenes as arylating reagents is the  $\alpha$ -amino arylation photoredox reaction, first identified by MacMillan and coworkers. 41 In this reaction, a photoredox cross-coupling between various cyanoarenes and amines resulted in range of α-amino aryl products, which are broadly useful in pharmaceutical synthesis. Recently, using the coupling of 1,4dicyanobenezene (1,4-DCB) and phenylpyrrolidine (NPP), we thoroughly interrogated the reaction using photochemical measurements, transient laser spectroscopy, and electrochemical methods and were able to identify several new mechanistic pathways and assign rate constants to the individual steps within the reaction (Scheme 1).<sup>42</sup> The reaction is initiated by electron transfer from a photoexcited Ir(ppy)<sub>3</sub> photocatalyst to give [1,4-DCB]<sup>-</sup> and [Ir(ppy)<sub>3</sub>]<sup>+</sup> (k<sub>quench</sub>). NPP does not participate in the quenching reaction as the  $k_a$  is on the order of  $10^3$ M<sup>-1</sup> s<sup>-1</sup>. Next, the oxidized photocatalyst is then regenerated by oxidizing NPP to give [NPP]\*+ (k<sub>ox</sub>), which is subsequently deprotonated to give [NPP] (k<sub>deprot</sub>). While this step has the smallest rate constant, kinetic modeling suggests that it is fast enough to outcompete recombination between the radicals (k<sub>rad recomb</sub> and k<sub>rad recomb2</sub>). Coupling between the radical anion and neutral radical (k<sub>couple</sub>), followed by loss of cyanide, gives the final product. Transient absorption spectroscopy (TAS) data revealed that deprotonation of [NPP]\*+ is the slowest step and also that [1,4-DCB].

undergoes pairing with a neutral 1,4-DCB molecule to form a radical ion pair, [1,4-DCB]2. However, kinetic modeling indicates that the external quantum yield (QY) of this reaction is not limited by the coupling chemistry, but by photons being lost to parasitic absorption of an NPP/DCB donor-acceptor complex as well as scattering by an insoluble sodium acetate base.

Figure 1. Cyanoarene coupling partners used in this study.

Implicit in the mechanism developed by this previous study is that given sufficient time the reaction should achieve product yields of 100%. In the case of 1,4-DCB that is largely accurate as we reported a product yield of 88% at 24 hr, which was in good agreement with the 96% yield obtained by MacMillan and coworkers. However, using a cyanoarene other than 1,4-DCB leads to markedly lower product yields, which cannot be explained by the mechanism in **Scheme** 1. This suggests a chemically irreversible unproductive step that was not identified in our previous report. In this study, we explore a wider

range of cyanoarene coupling partners (**Figure 1**) and observe reduced yields compared to 1,4-DCB, even after 96 hr of illumination. Analysis of the reaction mixtures demonstrates the formation of side products consistent with radical anion fragmentation, which is supported by electrochemical and computational studies on the stability of the radical anions. The trends in cyanoarene radical anion stability and overall product yield, are consistent with the selectivity of the reaction being influenced by the stability of the persistent cyanoarene radical anion.

### RESULTS AND DISCUSSION.

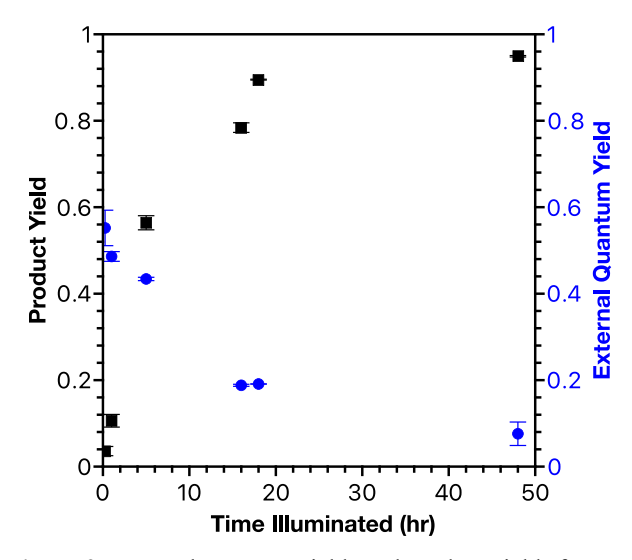
Steady-state photochemical studies. As a starting point, we determined the product yield (PY) and QY for the cross-coupling of NPP and our set of cyanoarene coupling partners (Table S1). Though our previous study utilized sodium acetate as the base in the reaction, in this study tetrabutylammonium acetate was used to remove scattering effects related to the base. Also, we note the external QY was measured, which is determined as the amount of product generated divided by the moles of incident photons. The concentration of photocatalyst is sufficiently high that it is capable of absorbing all incident photons. In addition, the cyanoarenes and NPP form

3

Scheme 1. Overall kinetic scheme with rate constants for the coupling of N-phenylpyrrolidine (NPP) and 1,4-dicyanobenzene (DCB). Red arrows indicate steps that are catalytically unproductive.

ground-state donor-acceptor complexes that parasitically absorb light but do not lead to productive photochemistry<sup>42</sup> (Figures S26-S30) The donor-acceptor complex also has little impact on the quenching as we measure a  $k_q$  of 1.92 x 10<sup>9</sup>  $M^{-1}$  s<sup>-1</sup> for DCB in a donor-acceptor complex with NPP. Thus, while we estimate ~40-45% of the incident photons go to the donor-acceptor complex, it is difficult to determine the value exactly. As a result, we prefer the use of external QY, which does not depend on knowing the exact number of photons absorbed by the photocatalyst.

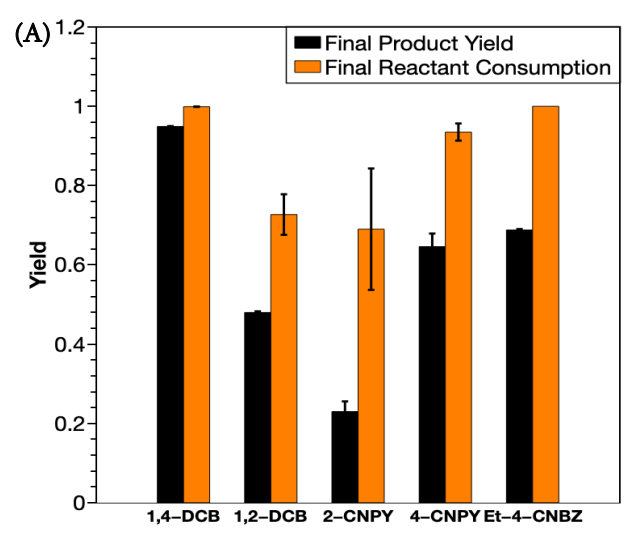
Figure 2 shows the plot of PY and QY for 1,4-DCB over 48 hr. Generally, the QY is greater than in our previous study (0.3 to 0.15) because of the use of a soluble base in this study, which eliminates scattering. When TBA acetate was used in our previous study, 1,4-DCB had an initial quantum yield of 0.52 at 0.5 hr, which is consistent with the results in Figure 1.<sup>42</sup> Also, in this study we extended the illumination time to 48 hr, which resulted in an increase of PY to 95%. As is typical for a photochemical reaction, the rate of product formation is controlled by the photon flux (Figures S35 and S36).



**Figure 2.** External quantum yields and product yields for cross-coupling reaction with 1,4-DCB.

Consistent with the observations of MacMillan and coworkers, we observe a decrease in PY when using the other cyanoarenes. **Figure 3a** shows the PY and percent cyanoarene consumption for all the cyanoarenes at the final measured time point. After 96 hr of illumination, Et-4-CNBZ had achieved complete cyanoarene

consumption, though the product yield was only 69%. 4-CNPY achieved nearly complete cyanoarene consumption within 48 hr but likewise exhibited a lower PY (65%). For 1,2-DCB, even after 90 hr of illumination, only 73% of the cyanoarene had been consumed for a PY of 48%. Finally, 2-CNPY achieved a maximum yield of 22% after 48 hr, with 69% of the cyanoarene



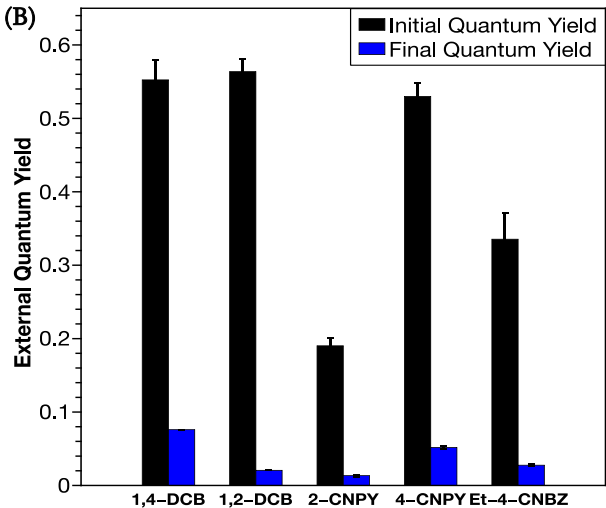


**Figure 3.** (A) Final PY and reactant conversions of cross-coupling reactions with cyanoarene substrates. (B) Initial (15 min) and final QY of cross-coupling reactions.

having been consumed. Illumination of the 2-CNPY for an additional 22 hr did not result in a statistically significant increase in the overall yield. Apart from 1,2-DCB, all of the PY were within 10% or less of the values reported by MacMillan and coworkers.<sup>41</sup> We also note that except for 1,4-DCB, there is a significant discrepancy between the overall PY and the amount of cyanoarene consumed. This is consistent with a chemically irreversible pathway that is absent or insignificant for 1,4-DCB.

The yield data collected in this current study allowed us to test a previous prediction about the impact of quenching on QY.<sup>42</sup> Kinetic modeling on the coupling of 1,4-DCB and NPP suggested that the rate constant for quenching (k<sub>q</sub>) could be decreased by two orders of magnitude relative to 1,4-DCB and have minimal impact on

the QY. To that end, we determined kq for each using Stern-Volmer methods cyanoarene (Supporting Information). Table 1 shows a significant variation in kq with a maximum value of 2.2 x 10<sup>9</sup> M<sup>-1</sup> s<sup>-1</sup> for 1,4-DCB and a minimum value of 2.1 x 10<sup>6</sup> M<sup>-1</sup> s<sup>-1</sup> for 2-CNPY. There is a rough correlation between the value of the kq and the standard reduction potential, E°, with more electron rich substrates showing smaller values of  $k_q$ . The initial QY yield (**Figure 3B**), however, does not show a dependence on kq, which is consistent with our predictions from kinetic modeling. For example, despite a nearly two orders of magnitude difference in k<sub>q</sub> for 1,4-DCB and 4-CNPY, they both exhibit nearly identical initial QY (0.55 and 0.53, respectively). The initial QY of 1,2-DCB (0.56) was also similar to 1,4-DCB and 4-CNPY despite it having a k<sub>q</sub> one order of magnitude lower than 1,4-DCB and one order of magnitude greater than 4-CNPY. Likewise, Et-4-CNBZ having the second largest kq has an initial QY of 0.34. 2-CNPY has the lowest  $k_q$  and the lowest initial QY of 0.19. Typical for a photochemical reaction, we observe a decrease in the OY over the course of the reaction (Figure **3B**). As with the initial QY, we do not observe a dependence of the final QY on kq. Overall, there is a general correlation between final QY and PY.

Table 1. Quenching Rate Constants and Standard Reduction Potentials for Cyanoarenes

	k <sub>q</sub> (M <sup>-1</sup> s <sup>-1</sup> )	E <sub>0</sub> (V v. NHE)
1,4-DCB	$2.2 \times 10^9$	-1.18
1,2-DCB	$9.3 \times 10^8$	-1.42
4-CNPY	$1.4 \times 10^7$	-1.87
2-CNPY	$2.1 \times 10^6$	-1.79
Et-4-CNBZ	1.6 x 10 <sup>9</sup>	-1.34

Finally, we note an unexpected observation for Et-4-CNBZ. Over the course of the illumination, quantitative NMR shows 100% consumption of Et-4-CNBZ after 48 hr of illumination, however, the PY for the coupling product with NPP continues to increase by 12%

over an additional 48 hr. Attempts to use ethyl-4-benzoate (*vide infra*) instead of Et-4-CNBZ did not result in product formation, which suggests an unknown reaction pathway that we are unable to identify at this time.

Stability of the cyanoarene radical anion. In analyzing the reaction mixtures, products were observed that were consistent with fragmentation of the cyanoarene radical anion. In order to identify these fragmentation products, gas chromatography-mass spectroscopy (GC-MS), <sup>1</sup>H NMR, and <sup>13</sup>C NMR were used. The GC-MS spectra for reactions using 1,2-DCB revealed one chromatographic peak at m/z 77 corresponding benzene (Figure S20). Further investigation into the <sup>1</sup>H NMR of 1,2 DCB reactions led to the identification of peaks that also corresponded with benzonitrile and benzene. In reactions with Et-4-CNBZ, a side product of ethyl benzoate was identified in both GC-MS and <sup>1</sup>H NMR spectra. Reactions with 4-CNPY and 2-CNPY exhibited GC-MS peaks at m/z at 79 indicating the presence of pyridine as a side product. (Figure S23).

To investigate the fragmentation of the cyanoarene radical anion, we turned computational and electroanalytical methods. Calculations demonstrated that while the free energies of reduction were all favorable, the fragmentation free energies are all uphill (Table 2). Overall, substitution and heteroatoms lead to opposite free energy trends in reduction and fragmentation. The largest free energies changes for reduction are for 1,4-DCB and 1,2-DCB then followed by Et-4-CNBZ, 4-CNPY, and 2-CNPY (Table 2). The subsequent fragmentations have the inverse trend, where 2-CNPY is the most favorable and 1.4-DCB is the least favorable. This trend is consistent with other studies regarding the reduction potential trends of other aromatic-type molecules. It has been observed that as reduction potentials become more positive, the rate of fragmentation increases.<sup>43</sup>

Fragmentation rates were determined from variable-rate cyclic voltammetry (CV). At slow scan rates, CVs for all of the coupling partners demonstrated some degree of irreversibility after reduction, with the 1,4-DCB only exhibiting a small amount of irreversibility. By varying the scan rate from .010 V/s to 1 V/s, a partial oxidation

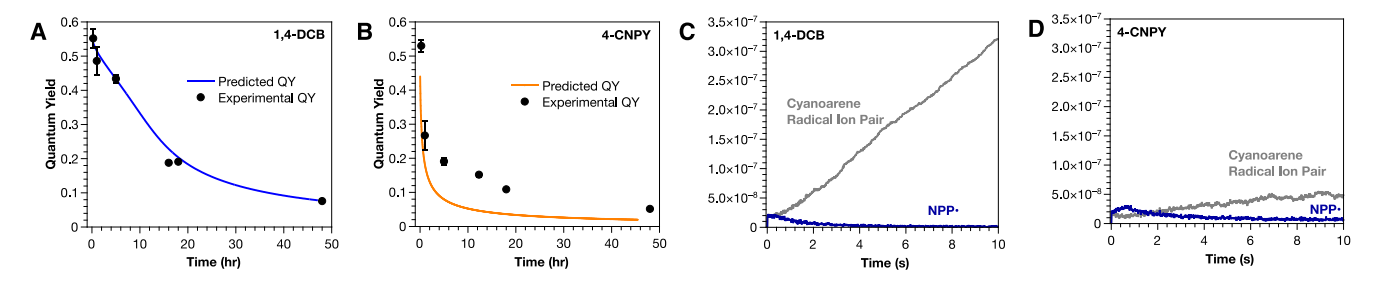
peak corresponding to the cyanoarene radical anion could be observed. Fits of the various CVs to an EC mechanism were then used to extract a value for k<sub>frag</sub>.(Table S2 and Figure S33)

Table 2.  $\Delta G_{red},$   $\Delta G_{frag},$  and  $k_{frag}$  for cyanoarenes

	ΔG <sub>red</sub> (kJ/mol)	ΔG <sub>frag</sub> (kJ/mol)	kfrag (s <sup>-1</sup> )
1,4-DCB	-277.23	176.51	$0.008 \pm 0.003$
1,2-DCB	-269.80	164.78	$0.011 \pm 0.003$
4-CNPY	-244.89	138.40	3 ± 1
2-CNPY	-228.65	125.65	$0.11 \pm 0.06$
Et-4- CNBZ	-264.65	169.70	$0.014 \pm 0.002$

The observed fragmentation rates are shown in **Table 2**. Fragmentation of 1,4-DCB was the slowest with  $0.008 \pm 0.003$  s<sup>-1</sup>, while 4-CNPY and 2-CNPY had the largest values of k<sub>frag</sub> with 3  $\pm$  1 s<sup>-1</sup> and 0.11  $\pm$  0.06 s<sup>-1</sup> respectively.  $k_{frag}$  for 1,2-DCB and Et-4-CNBZ were similar with values of  $0.011 \pm 0.003 \text{ s}^{-1}$  and  $0.014 \pm 0.002 \text{ s}^{-1}$ , respectively. The values of k<sub>frag</sub> in this study are comparable to k<sub>frag</sub> for some t-alkoxy radicals, where cleavage rates ranged from 0.003 to 1 s<sup>-1</sup>.<sup>44</sup> In contrast, the fragmentation of the cyanoarenes significantly slower than was reported fragmentation rates of aryl halides polyfluorinated benzoates, which have recorded rate constants spanning from 10<sup>4</sup> to 10<sup>9</sup> s<sup>-1</sup>. <sup>44,45</sup> The predicted trend of  $\Delta G_{frag}$  agrees well with the experimental k<sub>frag</sub> data. Namely, 1,4-DCB is the least favorable toward fragmentation while the cyanopyridines coupling partners are the most favorable towards fragmentation.

There is a much stronger correlation between the observed PY and  $k_{frag}$  than there is between PY and  $k_q$ . 1,4-DCB had an overall 95% percent yield with 99% reactant conversion. This is explained well since 1,4-DCB is the most stable of the cyanoarenes. With Et-4-CNBZ, the yield drops to 69% percent yield though 100% of the cyanoarene has been consumed. The other 30% of



**Figure 4.** Experimental QY for 1,4-DCB (A) and 4-CNPY (B) with predicted QY from kinetic modeling overlaid as well as the concentrations of cyanoarene radical ion pair and NPP• over the first 10s of the reaction for 1,4-DCB (C) and 4-CNPY (D).

Et-4-CNBZ was converted to fragmentation products in the reaction. Finally, 2-CNPY had a 23% percent yield with 69% of the cyanoarene consumed. The remaining 46% of the consumed 2-CNPY went into unproductive fragmentation pathways, as in the case of 4-CNPY. This production of fragmentation products explains the decrease in QY because some incident photons lead to an unproductive fragmentation event instead of generating the desired cross-coupled product.

Impact of cyanoarene radical anion stability on selectivity. In reactions where transient and persistent radicals are formed at similar rates, the cross-coupling product is the dominant product when the persistent radical effect (PRE) dominates. 46,47 The PRE occurs when the transient radical self-terminates  $(T \bullet + T \bullet \to T - T)$  and the persistent radical does not self-terminate or selfterminates at a much slower rate. In that case, the persistent and transient radicals are primarily consumed by the cross-coupling reaction  $(P \bullet + T \bullet \rightarrow P - T)$  because the concentration of the persistent radical builds up and favors the formation of the cross-coupling product over selftermination of the transient radical. However, in addition to the major cross-coupling product, other products such as T-H and P-H may be generated due to disproportionation.<sup>48</sup>

In the reaction with NPP, the NPP radical cation can undergo an α-cyanation to form 1-phenyl-2-pyrrolidinecarbonitrile.<sup>49</sup> This side product was observed by GC-MS in reactions with ET-4-CNBZ, 4-CNPY, and 1,2-DCB reactions. The <sup>13</sup>C NMR spectra for a 4-CNPY reaction also displayed peaks corresponding to the NPP-cyanation product, providing further evidence for this unproductive pathway. As this pathway will be common to all the cyanoarenes, we suggest the

contributing factor to the differences in yields is the stability of the cyanoarene persistent radical anions, in analogy with the PRE. Reactions with 1,4-DCB as the cyanoarene coupling partner are a good example of this since the cross-coupling product is generated with very high selectivity. On the other hand, reactions with the four other cyanoarene substrates do not demonstrate the same level of product selectivity, due to the formation of side products, such as pyridine. This explains why 1,4-DCB has high product selectivity and yields 95% versus 4-CNPY with 65% product yield and a nearly 100% cyanoarene consumption. As the cyanoarene radical anion becomes less stable, the likelihood of side products from fragmentation increases, thus decreasing the steady state of cyanoarene radical anion. In turn, the absolute rate of coupling between the NPP• and cyanoarene radical anion will decrease, allowing for more of the NPP• to form 1-phenyl-2-pyrrolidinecarbonitrile

To investigate this, we used kinetic modeling. As a starting point, we modeled the reaction between 1,4-DCB and NPP and added in a fragmentation step with a rate constant of 0.008 s<sup>-1</sup>. We also added a step for the reaction of the NPP• with -CN to form 1-phenyl-2pyrrolidinecarbonitrile. The rate constant for the formation of 1-phenyl-2-pyrrolidinecarbonitrile was varied until a good fit was achieved to the QY data for 1,4-DCB at  $3 \times 10^5 \,\mathrm{M}^{-1}\mathrm{s}^{-1}$  (Figure 4a). We then adjusted the model for 4-CNPY to account for lower the lower k<sub>q</sub>, slightly less parasitic light absorption by the donor-acceptor complex with NPP, and faster  $k_{frag}$ . All of the other parameters were left the same as with 1,4-DCB since the majority are already diffusion controlled and previous kinetic modeling suggests varying these parameters would have minimal impact on the reaction performance.<sup>42</sup> Though not quite as close as the match with 1,4-DCB, the match between the predicted QY and measured QY for 4-CNPY is nonetheless very good (**Figure 4b**). For the other cyanoarenes (**Figure S34**), the QY predicted by the kinetic modeling is satisfactorily close to the experimental QY for 1,2-DCB and Et-4-CNBZ but is an excellent match to the experimental QY for 2-CNPY.

The steady state concentrations of radical anion and pyrrolidinecarbonitrile predicted by the kinetic modeling provide several important insights into the coupling reaction. When looking at the first 10 seconds of the kinetic modeling there is a buildup results. 1-phenvl-2pyrrolidinecarbonitrile over the course of both reactions, with a more significant concentration in the reaction with 4-CNPY. Importantly, there is also a buildup of cyanoarene radical anion, modeled as the radical ion pair, during the reaction. For 1,4-DCB, at short times, both NPP• and the cyanoarene radical anion (in the form of a radical ion pair) are generated at the same rate before the steady-state concentration of NPP• decreases due to the formation of 1-phenyl-2pyrrolidinecarbonitrile (Figure 4c). The radical anion species continues to build up over the first 6 hours of the reaction to a maximum concentration of 35 µM. In the case of 4-CNPY, at short times there is little buildup of the radical anion species and the reaction never goes above a steady state concentration of 450 nM (Figure 4d). As a consequence, since the coupling step is a second order process dependent on the concentration of both species, the absolute rate of coupling will be faster with 1,4-DCB when compared to 4-CNPY. This is reflected the significantly higher undesired concentration of 1-phenyl-2pyrrolidinecarbonitrile generated in the case of 4-CNPY compared to 1,4-DCB (49 mM and 11 mM respectively). It is worth noting that the curves in Figures 4c and 4d match the predicted curve shapes and approximate timescales for persistent and transient radicals in reactions controlled by the PRE.<sup>47</sup>

### CONCLUSION.

The  $\alpha$ -amino arylation reaction analyzed in this study yields differing amounts of the cross-coupling product depending on which cyanoarene coupling partner reacts with NPP. In a previous

study we suggested the possibility of a breakdown pathway in this reaction, thus accounting for a decrease in product yield. Characterization of the post-illumination reaction solutions detected the formation of side products, providing evidence for unproductive pathways. alternate. We hypothesized that the diminished product selectivity is related to the stability of the cyanoarene radical anion. Experimental and computational studies supported the conclusion that cyanoarene coupling partners with increased rates of fragmentation from the radical anion exhibit decreased product selectivity.

Though the mechanism of this selectivity control differs from a classical example of the PRE, we suggest that it is nonetheless conceptually the same and represents a version of the PRE. Both the NPP• and cyanoarene radical anion are produced on nearly identical (< ms) timescales. While we do not observe evidence for self-termination of NPP• dimerization) we do observe the formation of 1phenyl-2-pyrrolidinecarbonitrile, represents a loss pathway for NPP. The reaction features the same selection pressure for the desired cross-coupling, namely the increase concentration of persistent radical species in comparison to the transient radical species. Finally, as in a classical demonstration of the PRE, the stability of the persistent radical species plays a key role in controlling the buildup of the persistent radical cross-coupling partner.

## EXPERIMENTAL SECTION.

Fac-tris(2-phenylpyridine) Iridium (III), 1,2dicyanobenzene, 1,4-dicyanobenzene, ethyl-4cyanobenzoate, 4-cyanopyridine, 2cyanopyridine, tetrabutylammonium acetate (TBA Acetate), N, N-dimethylacetamide (DMA), triphenylmethane, and technical grade 60 A° pore size silica gel were purchased from Millipore Sigma and used as received. N-phenylpyrrolidine was purchased from Fisher Scientific and used as received. Deuterated acetonitrile (acetonitrile-d<sub>3</sub>) purchased Cambridge from laboratories and used as received. Hexanes was purchased from Pharmco-Aaper and used as received. Ethyl-acetate was purchased from Macron Fine Chemicals and used as received. and used as received. HPLC grade methanol (≥99.9%) was purchased from Millipore Sigma and used as received.

Kinetics for the Rate of Fragmentation. All electrochemical experiments were performed using BioLogic SP-50 potentiostat, with 1 mm gold working electrode, pseudo-Ag/Ag+ reference electrode, and platinum coiled counter electrode, referenced to ferrocene as an internal standard in .100M TBNPF<sub>6</sub> in DMA as electrolyte. A water circulator jacketed single-cell electrochemical glassware was used, and the electrodes were inserted into a jacketed electrochemical cell using a septum to produce an airtight seal. Temperature control was maintained by using a PolyScience 6liter Analog Controller Refrigerated/Heated Circulating Bath apparatus. concentrations of 100 mM in electrolyte solution were used for all cyanoarene coupling partners, and cyclic voltammograms (CVs) from 0.10 mV/s - 5 V/s where possible. Slow scan rate CVs (10 mV/s - 1V/s) were fit using CVfit software supplied with the BioLogic EC-Lab based on an EC-type mechanism to values for k<sub>f</sub>.

**Ouantum** Yield **Product** and Yield Measurements. Argon was bubbled through the DMA for 30 minutes prior to each use. 0.5 mmol (1 equiv) cyanoarene, 2.5 µmol (0.005 equiv) Ir(ppy)<sub>3</sub>, 1 mmol (2 equiv) TBA acetate, 1.5 mmol (3 equiv) NPP, 2 mL DMA (2.218 mL total volume, 0.225 M cyanoarene) and a stirring flea were added to a clean borosilicate Starna Cells special optical glass Rectangular Spectrophotometer Cell screw top cap 10mm pathlength cuvette. The reaction solution was degassed with argon for an additional 45 minutes. The cuvette was placed on a stirring plate with a 3D printed cuvette holder 6.5 cm away from a collimated 415 nm LED (Thor Labs M415L4, full width half max of 12 nm  $\pm$  2 nm) and illuminated for 1-96 hours. The reaction solution was stirred for 30 minutes prior to illumination. The LED power was measured to 10.41 mW (14.65 mW/cm<sup>2</sup>) using a calibrated photodiode (Thor Labs S120C). No LED filters were used.

For reactions involving 2-cyanopyridine a 0.25 M stock solution was made under air-free

conditions in a glovebox. First, a 100 mL round bottom flask, a 250 mL round bottom flask, and two 25 mL volumetric flasks were thoroughly cleaned and dried in an oven overnight. 100 mL of DMA and 50 g molecular sieves were added to the 250 mL round bottom flask and degassed with nitrogen for 1 hour. In the glovebox, 0.6505 g (6.25 mmol) of 2-cyanopyridine was measured and added to one of the 25 mL volumetric flasks. The volumetric flask was filled up to the calibration mark with the degassed DMA using a beral pipet. This process was repeated with the second volumetric flask to afford 50 mL of 0.25 M 2-cyanopyridine in DMA. This stock solution degassed for 45 min and then 2.0 mL was added via syringe to a clean Starna Cells special optical glass Rectangular Spectrophotometer Cell with a screw top cap 10mm pathlength cuvette along with 0.00165 g (2.5 µmol, 0.005 equiv) Ir(ppy)<sub>3</sub>, 0.3016 g (1 mmol, 2 equiv) TBA acetate, and 0.218 g (1.5 mmol, 3 equiv) NPP. The reaction solution was degassed with argon for an additional 45 minutes. The cuvette was placed on a stirring plate with a 3D printed cuvette holder 6.5 cm away from a collimated 415 nm LED (Thor Labs M415L4, full width half max of 12 nm  $\pm$  2 nm) for 1-70 hours. The reaction solution was stirred for 30 minutes prior to illumination. The LED power was measured to 10.41 mW (14.65 mW/cm2) using a calibrated photodiode (Thor Labs S120C).

After illumination, 0.0611 g (0.25 mmol) of triphenylmethane was added to the solution and stirred for 30 minutes to ensure homogeneity. 175 uL of the reaction solution and 350 uL of acetonitrile-d3 were micropipetted into a Wilmad NMR tube (5 mm diameter, precision, 400 MHz frequency, 7 in. length). The sample was measured on a Bruker Avance III HD 400 and analyzed with Bruker TopSpin 4.1.0 software. <sup>1</sup>H NMR spectra were calibrated to a singlet at 1.97 ppm corresponding N,N-dimethylacetamide to hydrogens. Quantum yield and product yield were calculated following the formula provided in the SI.

Column Chromatography. Using a Pasteur pipet, silica gel, and a solvent system of 1:1 ethyl acetate and hexanes, column chromatography was carried out to separate the iridium photocatalyst from the reaction solution to perform gas-phase

mass spectroscopy (GC-MS). To prepare the Pasteur pipet, 5 g silica was dissolved in approximately 25 mL of the solvent system. Once homogenized, the slurry was pipetted into the Pasteur pipet and allowed to settle. Subsequently, the post-illumination reaction solutions were pipetted into the pipet column, and the purified solutions were collected for GC-MS analysis.

Gas Phase Mass Spectroscopy. To prepare the sample for GC-MS analysis, one drop of the purified post-illumination reaction solution was dissolved in 1 mL of HPLC-grade methanol (≥99.9%). This mixture was filtered through a syringe filter using a 3 mL plastic syringe and collected in a 2 mL GC-MS glass vial. GC-MS spectra were measured on a Shimadzu GC-2010 Plus instrument.

Density Functional Theory. The relaxed ground state electronic structure of the neutral and reduced five coupling partners and their electrochemical fragments were optimized using the widely used M06-L functional with empirical dispersion (D3) 1 in conjunction with standard Gaussian type orbital (GTO) basis sets of triple-ζ quality, 6-311G(d,p), with a complete polarizable continuum model (PCM) solvent description for DMA. All calculations were performed using the Gaussian16 program.2 The fully optimized minima were run with no symmetry constraints applied and confirmed by no imaginary frequencies. All energies are thermally corrected Gibbs free energies, with redox potentials calculated via the Nernst equation.

# ASSOCIATED CONTENT.

• Data Availability Statement The data underlying this study are available in the published article and its Supporting Information .

# SUPPORTING INFORMATION STATEMENT.

Detailed procedures for kinetic modeling, NMR data of reaction mixtures, GCMS of side products, detailed quantum yield and product yield data for all coupling partners, product yield as a function of LED power and reagent loading, Stern-Volmer

measurements for rates of quenching of coupling partners and donor-acceptor complex, UV-Vis analysis of donor-acceptor complex

### **AUTHOR INFORMATION.**

# **Corresponding Authors**

John R. Swierk – Department of Chemistry, State University of New York Binghamton, 4400 Vestal Parkway East, Binghamton, New York 13902, Email: jswierk@binghamton.edu

Lisa Fredin- Department of Chemistry, Lehigh University, 6 E. Packer Ave, Seeley G. Mudd, Bethlehem, PA 18015

Email: laf218@lehigh.edu

### **Authors**

**Bernard G. Stevenson -** Department of Chemistry, State University of New York Binghamton, 4400 Vestal Parkway East, Binghamton, New York 13902.

Cameron Gironda- Department of Chemistry, State University of New York Binghamton, 4400 Vestal Parkway East, Binghamton, New York 13902.

Eric Talbott- Department of Chemistry, State University of New York Binghamton, 4400 Vestal Parkway East, Binghamton, New York 13902.

**Nora L. Burnett-** Department of Chemistry, State University of New York Binghamton, 4400 Vestal Parkway East, Binghamton, New York 13902.

**Victoria Kompanijec-** Department of Chemistry, State University of New York Binghamton, 4400 Vestal Parkway East, Binghamton, New York 13902.

Roman Nakhamiyayev- Department of Chemistry, State University of New York Binghamton, 4400 Vestal Parkway East, Binghamton, New York 13902.

**Amanda Prascsak-**Department of Chemistry, Lehigh University, 6 E. Packer Ave, Seeley G. Mudd, Bethlehem, PA 18015

ACKNOWLEDGEMENTS. This work was supported by the National Science Foundation (Award Number CHE-2047492). BGS, CG, and ET, and NLB also thank the Department of Chemistry at Binghamton University for summer fellowships. Portions of this research were conducted with research computing resources provided by the TG-CHE190011 allocation from Extreme Science and Engineering Discovery Environment (XSEDE), which is supported by National Science Foundation grant number ACI-1548562 and the NSF CC\* Compute program (OAC-2019035) for funding to increase computing resources at Lehigh University.

### REFERENCES.

- (1) Shaw, M. H.; Twilton, J.; MacMillan, D. W. C. Photoredox Catalysis in Organic Chemistry. *J. Org. Chem.* **2016**, *81*, 6898-6926.
- (2) Wang, C.; Dixneuf, P. H.; Soule, J. Photoredox Catalysis for Building C-C Bonds from C(sp<sup>2</sup>)-H Bonds. *Chem. Rev.* **2018**, *118*, 7532-7585.
- (3) Rueda-Becerril, M.; Mahe, O.; Drouin, M.; Majewski, M. B.; West, J. G.; Wolf, M. O.; Sammis, G. M.; Paquin, J. Direct C-F Bond Formation Using Photoredox Catalysis. *J. Am. Chem. Soc.* **2014**, *136*, 2637-2641.
- (4) Holmberg-Douglas, N.; Nicewicz, D. A. Photoredox-Catalyzed C-H Functionalization Reactions. *Chem. Rev.* **2022**, *122*, 1925-2016.
- (5) Ganley, J. M.; Murray, P. R. D.; Knowles, R. R. Photocatalytic Generation of Aminium Radical Cations for C-N Bond Formation. *ACS Catal.* **2020**, *10*, 11712-11738.
- (6) Wang, X.; Xia, C.; Wu, L. Visible-Light-Promoted Photoredox Dehydrogenative Coupling of Phosphines and Thiophenols. *Organic Letters* **2020**, *22*, 7373-7377.
- (7) Allen, A. R.; Noten, E. A.; Stephenson, C. R. J. Aryl Transfer Strategies Mediated by Photoinduced Electron Transfer. *Chem. Rev.* **2022**, 2695–2751.

- (8) Wang, H.; Tian, Y.-M.; König, B. Energyand Atom-Efficient Chemical Synthesis with Endergonic Photocatalysis. *Nat. Rev. Chem.* **2022**, 6 (10), 745–755.
- (9) Medina, E.; Pinter, B. Electron Density Difference Analysis on the Oxidative and Reductive Quenching Cycles of Classical Iridium and Ruthenium Photoredox Catalysis. *J. Phys. Chem. A.* **2020**, *124*, 4223-4234.
- (10) Dai, P.; Ma, J.; Huang, W.; Chen, W.; Wu, N.; Wu, S.; Li, Y.; Cheng, X.; Tan, R. Photoredox C-F Quaternary Annulation Catalyzed by a Strongly Reducing Iridium Species. *ACS Catal.* **2018**, *8*, 802-806.
- (11) Narayanam, J. M; Tucker, J. W.; Stephenson, C. R. J. Electron-Transfer Photoredox Catalysis: Development of a Tin-Free Reductive Dehalogenation Reaction. *J. Am. Chem. Soc.* **2009**, *131*, 8756-8757.
- (12) Nicewicz, D. A.; MacMillan, D. W. C. Merging Photoredox Catalysis with Organocatalysis: The Direct Asymmetric Alkylation of Aldehydes. *Science* **2008**, *322*, 77-80.
- (13) Ischay, M. A.; Anzovino, M. E.; Du, J.; Yoon, T. P. Efficient Visible Light Photocatalysis of [2+2] Enone Cycloadditions. *J. Am. Chem. Soc.* **2008**, *130*, 12886-12887.
- (14) Arias-Rotondo, D. M.; McCusker, J. K. The Photophysics of Photoredox Catalysis: A Roadmap for Catalyst Design. *Chem. Soc. Rev.* The Royal Society of Chemistry **2016**, 5803–5820.
- (15) Romero, N. A.; Nicewicz, D. A. Organic Photoredox Catalysis. *Chem. Rev.* **2016**, 10075–10166.
- (16) Soto, X. L.; Swierk, J. R. Using Lifetime and Quenching Rate Constant to Determine Optimal Quencher Concentration. *ACS Omega* **2022**, *7* (29), 25532–25536.
- (17) Rossi-Ashton, J. A.; Clarke, A. K.; Unsworth, W. P.; Taylor, R. J. K. Phosphoranyl Radical Fragmentation Reactions Driven by Photoredox Catalysis. *ACS Catal.* **2020**, **10**, 7250-7261.
- (18) Matsui, J. K.; Lang, S. B.; Heitz, D. R.; Molander, G. A. Photoredox-Mediated Routes to Radical: The Value of Catalytic Radical Generation in Synthetic Methods Development. *ACS Catal.* **2017**, *7*, 2563-2575.

- (19) Costentin, C.; Robert, M.; Saveant, J. Fragmentation of Aryl Halide  $\pi$  Anion Radicals. Bending of the Cleaving Bond and Activation vs Driving Force Relationships. *J. Am. Chem. Soc.* **2004**, *126*, 16051-16057.
- (20) Zhang, N.; Samanta, S. R.; Rosen, B. M.; Percec, V. Single Electron Transfer in Radical Ion and Radical-Mediated Organic, Materials and Polymer Synthesis. *Chem. Rev.* **2014**, *114*, 5848-5958.
- (21) Carsky, P.; Zahradnik, R. Radicals: Their Molecular Orbitals, Properties, and Reactivity. *Acc. Chem. Res.* **1976**, *9*, 407-411.
- (22) Haring, M.; Perez-Ruiz, R.; Jacobi, A.; Diaz Diaz, D. Intragel photoreduction of aryl halide by green-to-blue upconversion under aerobic conditions. *Chem. Commun.* **2015**, *51*, 16848-16851.
- (23) Qvortrup, K.; Rankic, D. A.; MacMillan, D. W. C. A General Strategy for Organocatalytic Activation of C-h Bonds via Photoredox Catalysis: Direct Arylation of Benzylic Ethers. *J. Am. Chem. Soc.* **2014**, *136* (2), 626–629.
- (24) Cuthbertson, J. D.; MacMillan, D. W. C. The Direct Arylation of Allylic Sp3 C-H Bonds via Organic and Photoredox Catalysis. *Nature* **2015**, *519* (7541), 74–77.
- (25) Spielvogel, E. H.; Stevenson, B. G.; Stringer, M. J.; Hu, Y.; Fredin, L. A.; Swierk, J. R. Insights into the Mechanism of an Allylic Arylation Reaction via Photoredox-Coupled Hydrogen Atom Transfer. *J. Org. Chem.* **2022**, *87* (1), 223–230.
- (26) Georgiou, E.; Spinnato, D.; Chen, K.; Melchiorre, P. Switchable Photocatalysis for the Chemodivergent Benzylation of 4-Cyanopyridines. *Chem. Sci.* **2022**, *13* (27), 8060–8064.
- (27) Xu, C.; Shen, F. Q.; Feng, G.; Jin, J. Visible-Light-Induced α-Amino C-H Bond Arylation Enabled by Electron Donor-Acceptor Complexes. *Org. Lett.* **2021**, *23* (10), 3913–3918.
- (28) Yan, C.; Li, L.; Liu, Y.; Wang, Q. Direct and Oxidant-Free Electron-Deficient Arylation of N-Acyl-Protected Tetrahydroisoquinolines. *Org. Lett.* **2016**, *18* (18), 4686–4689.
- (29) Natarajan, P.; Manjeet; Muskan; Brar, N. K.; Jot Kaur, J. Visible Light Photoredox Catalysis: Conversion of a Mixture of Thiophenols and Nitriles into 2-Substituted

- Benzothiazoles: Via Consecutive C-S and C-N Bond Formation Reactions. *Org. Chem. Front.* **2018**, *5* (9), 1527–1531.
- (30) Lipp, B.; Lipp, A.; Detert, H.; Opatz, T. Light-Induced Alkylation of (Hetero)Aromatic Nitriles in a Transition-Metal-Free C-C-Bond Metathesis. *Org. Lett.* **2017**, *19* (8), 2054–2057.
- (31) Walker, M. M.; Koronkiewicz, B.; Chen, S.; Houk, K. N.; Mayer, J. M.; Ellman, J. A. Highly Diastereoselective Functionalization of Piperidines by Photoredox-Catalyzed α-Amino C-H Arylation and Epimerization. *J. Am. Chem. Soc.* **2020**, *142* (18), 8194–8202.
- (32) Lipp, B.; Nauth, A. M.; Opatz, T. Transition-Metal-Free Decarboxylative Photoredox Coupling of Carboxylic Acids and Alcohols with Aromatic Nitriles. *J. Org. Chem.* **2016**, *81* (15), 6875–6882.
- (33) Nicastri, M. C.; Lehnherr, D.; Lam, Y. H.; Dirocco, D. A.; Rovis, T. Synthesis of Sterically Hindered Primary Amines by Concurrent Tandem Photoredox Catalysis. *J. Am. Chem. Soc.* **2020**, *142* (2), 987–998.
- (34) Speckmeier, E.; Fischer, T. G.; Zeitler, K. A Toolbox Approach To Construct Broadly Applicable Metal-Free Catalysts for Photoredox Chemistry: Deliberate Tuning of Redox Potentials and Importance of Halogens in Donor–Acceptor Cyanoarenes. *J. Am. Chem. Soc.* **2018**, *140*, 15353-15365.
- (35) Alsam, A. A.; Aly, S. W.; Usman, A.; Parida, M. R.; Del Gobbo, S.; Alarousu. E.; Mohammed, O. F. Bimolecular Excited-State Electron Transfer with Surprisingly Long-Lived Radical Ions. *J. Phys. Chem. C* **2015**, *119*, 21896-21903.
- (36) Chowdhury, S.; Heinis, T.; Kebarle, P. Radical Anions, Electron Affinities of Benzene, Napthalene, and Anthracene Having the Substituents CHO, CN, and NO<sub>2</sub>. *J. Am. Chem. Soc.* **1986**, *108*, 4662-4663.
- (37) Yildiz, A.; Sertel, M.; Gambert, R.; Baumgartel, H. On the Stabilities of the Anion Radicals, Dianions and Dimerdianions of Benzenedicarbonitriles. *Electrochimica Acta*. **1988**, *33*, 169-170.
- (38) Nakajima, K.; Nojima, S.; Sakata, K.; Nishibayashi, Y. Visible-Light-Mediated Aromatic Substitution Reactions of Cyanoarenes with 4-Alkyl-1,4-dihydropyridines through

- Double Carbon–Carbon Bond Cleavage. *Chem. Cat. Chem.* **2016**, *8*, 1028-1032.
- (39) Bilkis, I. I.; Vaganova, T. A.; Panteleeva, E. V.; Salnikov, G. E.; Tananakin, A. P.; Mamatyuk, V. I.; Shteingarts, V. D. Anionic products of the two-electron reduction of aromatic nitriles in liquid ammonia. *J. Phys. Org. Chem.* **1994**, *7*, 153–161.
- (40) Vaganova, T. A.; Yuferov, P. S.; Goryunov, L. I.; Panteleeva, E. V.; Sal'nikov, G. E.; Shchegoleva, L. N.; Mamatyuk, V. I.; Shteingarts, V. D. Reductive activation of arenes. 20. Anionic products of two-electron reduction of tolunitriles in liquid ammonia: The nature and electronic structure. *Russ. Chem. Bull.* **2006**, 55, 976–980.
- (41) McNally, A.; Prier, C. K.; MacMillan, D. W. C. Discovery of an α-Amino C-H Arylation Reaction Using the Strategy of Accelerated Serendipity. *Science* **2011**, *334*, 1114–1117.
- (42) Stevenson, B. G.; Spielvogel, E. H.; Loiaconi, E. A.; Wambua, V. M.; Nakhamiyayev, R. V.; Swierk, J. R. Mechanistic Investigations of an α-Aminoarylation Photoredox Reaction. *J. Am. Chem. Soc.* **2021**, *143*(23), 8878–8885.
- (43) Andrieux, C. P.; Saveant, J. M.; Zann, D. Relationship Between Reduction Potential and Anion Radical Cleavage Rates in Aromatic Molecules. *New J. Chem.* **1984**, *8*, 107-116.
- (44) Kochi, J. Chemistry of Alkoxy Radical: Cleavage Reactions. *J. Am. Chem, Soc.* **1962**, *84*, 1193-1197.
- (45) Konovalov, V. V.; Laev, S. S.; Beregovaya, I. V.; Shchegoleva, L. N.; Shteingarts, V. D.; Tsvetkov, Y. D.; Bilkis, I. Fragmentation of Radical Anions of Polyfluorinated Benzoates. *J. Phys. Chem. A.* **2000**, *104*, 352-361.
- (46) Takeda, N.; Poliakov, P. V.; Cook, A. R.; Miller, J. R. Faster Dissociation: Measured Rates and Computed Effects on Barriers in Aryl Halide Radical Anions. *J. Am. Chem. Soc.* **2004**, *126* (13), 4301–4309.
- (47) Leifert, D.; Studer, A. The Persistent Radical Effect in Organic Synthesis. *Angew. Chem. Int. Ed.* **2020**, *59*, 74-108.
- (48) Fischer, H. The Persistent Radical Effect: A Principle for Selective Radical Reactions and Living Radical Polymerizations. *Chem. Rev.* **2001**, *101*, 3581-3610.

(49) Liu, W.; Ma, Y.; Yin, Y.; Zhao, Y. Anodic Cyanation of 1-Arylpyrrolidines. *Bull. Chem. Soc. Jpn.* **2006**, *79* (4), 577–579